AIAA JOURNAL
Vol. 39, No. 10, October 2001

Gibbs-Phenomenon-Free Fourier Series for Vibration and Stability of Complex Beams

S. C. Fan* and D. Y. Zheng†
Nanyang Technological University, Singapore 639798, Republic of Singapore
and
F. T. K. Au‡
University of Hong Kong, Hong Kong, People's Republic of China

The Gibbs phenomenon in Fourier series has long been recognized as a drawback in its applications, in particular when it is used to represent a function having discontinuities. One category, namely, intrinsic discontinuities, could be derived from the nature of the physical problems. Another, namely, inherent discontinuities, is created undesirably through the employment of Fourier series. To alleviate these drawbacks, two techniques are developed. The first aims at eliminating the inherent discontinuities. The size of the original domain $[0, l]$ is first doubled with a virtual function φ_0 defined over the neighboring domain $[-l, 0]$. The augmented domain $[-l, l]$ is then further extended periodically. The virtual function $\varphi_0(y)$ is chosen so that continuities are achieved at $y = 0, \pm l, \pm 2l, \ldots$. Consequently, no Gibbs phenomena will occur at the boundaries. The second aims at reproducing the intrinsic discontinuities in the representation function by incorporating piecewise cubic polynomials into the Fourier base function. The enlarged basis function, namely, the Gibbs-phenomenon-free-Fourier-series function, is able to represent accurately any specific boundary conditions and interior intrinsic discontinuous conditions. Examples of vibration and buckling analysis of complex beams show that the present method is versatile, accurate, and efficient.

Nomenclature

$A_{jl}(y)$, $B_{jl}(y)$	=	Hermitian interpolation function associated with point j, $j = 2, \ldots, Q+1$ [for the $(j-1)$th segment]
$A_{jr}(y)$, $B_{jr}(y)$	=	Hermitian interpolation function associated with point j, $j = 1, 2, \ldots, Q$ (for the jth segment)
c_j	=	equivalent flexibility coefficient of a crack of depth a_j, $j = 2, \ldots, Q$
$\boldsymbol{H}_{jl}(y)$	=	row vector of the Hermitian interpolation functions $A_{jl}(y)$, $B_{jl}(y) - 1 \times 2$; $j = 2, \ldots, Q+1$
$\boldsymbol{H}_{jr}(y)$	=	row vector for the Hermitian interpolation functions $A_{jr}(y)$, $B_{jr}(y) - 1 \times 2$; $j = 1, 2, \ldots, Q$
h_i	=	length of an ith segment, $i = 1, 2, \ldots, Q$
I_j	=	moment of inertial of cross section of a jth segment, $j = 1, 2, \ldots, Q$
$\boldsymbol{K}_G$	=	geometrical stiffness matrix
$\boldsymbol{K}_1$	=	bending stiffness matrix for a beam
$\boldsymbol{K}_2$	=	rotational stiffness matrix for a massless rotational spring used to model a crack
L_j, L'_j	=	value and first derivative of the function $\tilde{Y}_m(y)$ at point y_j^- (left-hand side of y_j), $j = 2, \ldots, Q+1$
l	=	length of a beam
$\boldsymbol{M}$	=	mass matrix for a beam
Q	=	number of segments comprising a beam
$\boldsymbol{q}(t)$	=	column vector of $q_m(t) - R \times 1$
$q_m(t)$	=	generalized coordinates for a beam, $m = 1, 2, \ldots, R$
R	=	total number of terms used for an assumed mode, $2r$
R_j, R'_j	=	value and first derivative of the function $\tilde{Y}_m(Y)$ at point y_j^+ (right-hand side of y_j), $j = 1, 2, \ldots, Q$
r	=	order of a Fourier series
$w(y, t)$	=	deflection of a beam at location y and time t
$w_0(y)$	=	augmented function defined over the domain $[-l, l]$
$\boldsymbol{Y}(y)$	=	row vector of $Y_m(y) - 1 \times R$
$Y_m(y)$	=	Gibbs-phenomenon-free Fourier series, $m = 1, 2, \ldots, R$
$\bar{Y}_m(y)$	=	Fourier base function, $m = 1, 2, \ldots, R$
$\tilde{Y}_m(y)$	=	piecewise cubic polynomial function, $m = 1, 2, \ldots, R$
y_i	=	locations of interior intrinsic discontinuities, $i = 1, 2, \ldots, Q+1$
δ_{jl}	=	column vector for $L_j, L'_j - 2 \times 1$; $j = 2, \ldots, Q+1$
δ_{jr}	=	column vector for R_j and $R'_j - 2 \times 1$, $j = 1, 2, \ldots, Q$
$\varphi_0(y)$	=	virtual function constructed over the domain $[-l, 0]$
ω_0	=	Fourier basic frequency

I. Introduction

THE Fourier series has been used extensively in solving many mathematical and engineering problems. It can approach any smooth function effectively. On the other hand, its drawback has long been recognized. For a function with discontinuities, it can never be well represented by a continuous Fourier series function. It fluctuates in the vicinity of the discontinuity and converges to the average value of the jump. This is known as the Gibbs phenomenon.[1–8] For a complex beam, the discontinuities can be due to the existence of interior open cracks, abrupt changes of cross sections, or spanning over rigid supports. These discontinuities exist in the physical problem and so they are called intrinsic discontinuities. On the other hand, undesirable additional discontinuities are created from the employment of the Fourier series. Accordingly, they are called inherent discontinuities. They occur at the boundaries of the domain due to the inability of the Fourier series in simulating all kinds of boundary conditions. In both cases, Gibbs phenomena will inevitably occur at the locations of discontinuity. These undesired Gibbs phenomena hinder the versatility of the Fourier series and limit its applications.

To alleviate these drawbacks, two techniques are developed and presented in this paper. The first is developed to eliminate the inherent discontinuities. The original domain $[0, l]$ is first augmented to $[-l, l]$ with a virtual function φ_0 defined over the domain $[-l, 0]$. The augmented domain $[-l, l]$ is then further extended periodically to $(-\infty, +\infty)$. The virtual function $\varphi_0(y)$ is chosen so that continuities are achieved at $y = 0, \pm l, \pm 2l, \ldots$. As such, the Fourier series representation with a period $T = 2l$ over the extended domain $(-\infty, +\infty)$ will be free of Gibbs phenomena at $y = 0, \pm l, \pm 2l, \ldots$.

Received 18 November 2000; revision received 29 March 2001; accepted for publication 10 April 2001.

*Associate Professor, School of Civil and Structural Engineering; cfansc@ntu.edu.sg.
†Research Fellow, School of Civil and Structural Engineering; cdyzheng@ntu.edu.sg.
‡Associate Professor, Department of Civil Engineering, Pokfulam Road; hrecatk@hku.hk.

The second technique is to reproduce the intrinsic discontinuities in the representation function. It can be achieved easily by incorporating piecewise cubic polynomials into the Fourier base function. Consequently, the combined function can represent accurately any specific boundary conditions and any interior intrinsic discontinuous conditions as well. The final form of the representation function is called the Gibbs-phenomenon-free-Fourier-series (GPFFS) function. It forms the basis for deriving the vibration and/or buckling modes of a complex beam. In addition, the order of continuity of the GPFFS function can be varied at different locations of discontinuity. If it is C^0 continuous, an open crack can be simulated; if it is C^1 continuous, an abrupt change of cross section in a beam can be represented accurately; if it is C^2 continuous, a rigid-support condition can be reproduced. Of course, it could remain C^3 continuous. The discontinuities are dealt with in a unified manner.

Alternative approaches were reported in Refs. 9 and 10. They deal with the occurrence of open cracks in prismatic beams or abrupt changes of cross sections in stepwise prismatic beams. The governing differential equations for each prismatic segment are first set up and then solved segmentally. Their methods are good but not unified and can hardly be used for general nonprismatic beams. Using the present GPFFS function, unified formulas can be easily obtained. It allows the nonuniform beams be solved in the same manner as that for uniform beams. Furthermore, once the GPFFS function is defined, the remaining procedures in the vibration/buckling analysis of a complex beam will be the same as those of a simple beam. Subsequently, the existence of discontinuities will be taken care of automatically.

Recently, Au et al.[11] employed a kind of modified beam-vibration function to solve the vibration and buckling problems of a beam with abrupt changes of cross sections, but not beams having open cracks. Compared to the method in Ref. 11, the present method is more general and powerful.

II. Construction of GPFFS Functions

A. Fourier Base Function

Figure 1 shows an Euler beam with $(Q-1)$ interior intrinsic discontinuities at locations $y = y_j$, $j = 2, 3, \ldots, Q$. It divides the beam into Q segments. The discontinuity could be due to the existence of open cracks, abrupt changes of cross sections, or intermediate rigid supports.

The deflection of the beam at an arbitrary location y and time t can be expressed as

$$w(y,t) = \sum_{m=1}^{R} q_m(t) Y_m(y) = \boldsymbol{Y}(y)\boldsymbol{q}(t) \tag{1}$$

where

$$\boldsymbol{Y}(y) = [Y_1(y) \quad Y_2(y) \quad \cdots \quad Y_R(y)] \tag{2}$$

$$\boldsymbol{q}(t) = [q_1(t) \quad q_2(t) \quad \cdots \quad q_R(t)]^T \tag{3}$$

in which $Y_m(y)$ are the assumed vibration (or buckling) modes of the beam and $q_m(t)$ are the corresponding generalized coordinates for the beam.

The Fourier series has long been a convenient tool for both mathematicians and engineers. They use a standard Fourier series with a period $T = l$ to describe deflection or other physical phenomena. It represents a function $w(y, t_0)$ for a specific time t_0 over a domain $[0, l]$. However, Gibbs phenomena occur at the boundaries ($y = 0$ and $y = l$) due to the existence of discontinuity conditions (Fig. 2).

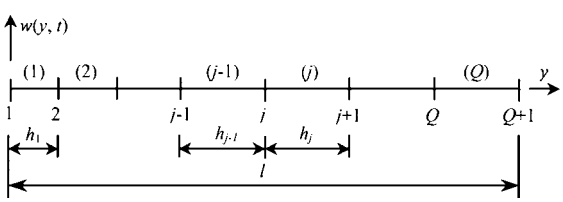

Fig. 1 Beam with $(Q-1)$ interior intrinsic discontinuities at $y = y_2, \ldots, y_Q$.

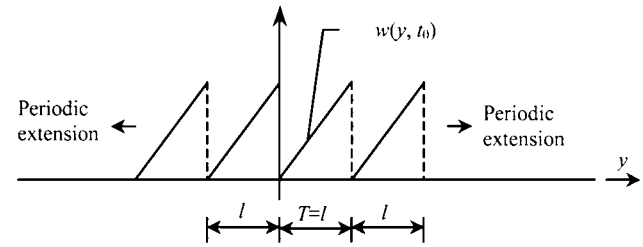

Fig. 2 Usual way of periodic extension of a function defined over a domain of $(0, l)$.

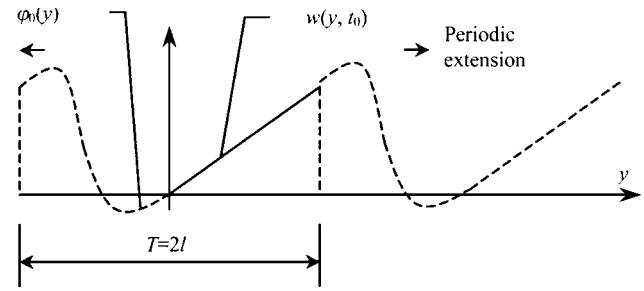

Fig. 3 New way of periodic extension of a function defined over the domain of $(0, l)$.

These discontinuities are due to the inherent direct periodic extension of the function $w(y, t_0)$. For example, the function $w(y, t_0)$ plotted in Fig. 2 is taken a simple form of a straight line.

To subdue the undesired Gibbs fluctuations, one can first construct a virtual function $\varphi_0(y)$ over the left neighboring domain $[-l, 0]$ so that a new function $w_0(y)$ over the augmented domain $[-l, l]$ is defined as follows (Fig. 3):

$$w_0(y) = \begin{cases} \varphi_0(y) & \text{for} \quad y \in [-l, 0] \\ w(y, t_0) & \text{for} \quad y \in [0, l] \end{cases} \tag{4}$$

The virtual function $\varphi_0(y)$ is chosen so that continuities are achieved at $y = 0$, that is, $\varphi_0^{(q)}(y)|_{y=0} = w^{(q)}(y, t_0)|_{y=0}$ for all degrees of derivative q ($q = 0, 1, 2, \ldots, \infty$). In addition, cyclic continuities are also achieved at the two ends ($y = \pm l$) so that $\varphi_0^{(q)}(y)|_{y=-l} = w^{(q)}(y, t_0)|_{y=l}$ for all degrees of derivative q ($q = 0, 1, 2, \ldots, \infty$). The augmented domain $[-l, l]$ is then further extended periodically to $(-\infty, +\infty)$. One can realize that the virtual function $\varphi_0(y)$ was chosen so that continuities are achieved at $y = 0, \pm l, \pm 2l, \ldots$. Consequently, the augmented function $w_0(y)$ with a period $T = 2l$ over the extended domain $(-\infty, +\infty)$ will be free of Gibbs phenomena at $y = 0, \pm l, \pm 2l, \ldots$. Subsequently, we can have the Fourier expansion[7] in the extended domain $(-\infty, +\infty)$

$$w(y, t_0) \sim \frac{a_0}{2} + \sum_{i=1}^{\infty} (a_i \cos i\omega_0 y + b_i \sin i\omega_0 y), \quad \text{where} \quad \omega_0 = \frac{\pi}{l} \tag{5}$$

in which ω_0 is the basic frequency of the Fourier series. This Fourier series representation will no longer exhibit Gibbs phenomena at $y = 0$ and $y = l$. Note that, when solving a real practical problem, there is no need to construct specifically the virtual function. This is because all subsequent numerical calculations are carried out over the original domain only. Therefore, the extended Fourier expansion can be conveniently taken as the virtual function.

To illustrate the success of eliminating the Gibbs phenomena at the boundaries ($y = 0$ and $y = l$), let us consider a cantilever beam. The problem is to find its natural frequencies. The boundary conditions at $y = 0$ is clamped, whereas at $y = l$, it is free. The length, width, and depth of the beam are $l = 0.8$ m (2.62 ft), $b = 0.02$ m (0.066 ft), and $h = 0.02$ m (0.066 ft), respectively. Young's modulus, Poisson's ratio, and mass density are $E = 210$ GPa (30.46E6 psi), $\mu = 0.33$, and $\rho = 7800$ kg/m^3 (15.13 slug/ft^3), respectively. The

Table 1 Dimensionless frequencies of a cantilever beam: $\beta_j = L\sqrt[4]{(\rho A\omega_j^2/EI)}$

	j									
ω_0	1	2	3	4	5	6	7	8	9	10
$0.5\pi/L$	1.8751	4.6940	7.8545	10.9948	14.1356	17.2759	20.4159	23.5600	26.9233	30.5656
$0.6\pi/L$	1.8751	4.6940	7.8545	10.9948	14.1356	17.2759	20.4157	23.5545	26.7026	29.9653
$0.7\pi/L$	1.8751	4.6941	7.8548	10.9955	14.1372	17.2787	20.4203	23.5618	26.7063	29.7811
$0.8\pi/L$	1.8751	4.6941	7.8548	10.9955	14.1372	17.2787	20.4203	23.5618	26.7032	29.8422
$0.9\pi/L$	1.8751	4.6941	7.8548	10.9955	14.1372	17.2787	20.4203	23.5619	26.7034	29.8450
$1.0\pi/L$	1.8751	4.6941	7.8548	10.9955	14.1372	17.2787	20.4203	23.5619	26.7034	29.8450
$1.25\pi/L$	1.8751	4.6941	7.8548	10.9955	14.1372	17.2787	20.4203	23.5619	26.7034	29.8450
$1.5\pi/L$	1.8856	4.6963	7.8550	10.9965	14.1372	17.2780	20.4204	23.5637	26.7036	29.8478
$1.75\pi/L$	3.5827	6.4307	8.7972	11.8846	14.4177	17.8137	20.5123	23.9729	26.7375	30.2030
$2.0\pi/L$	4.7302	8.0205	10.9975	14.4585	17.2862	20.9164	23.5809	27.3981	29.8838	33.9080
Exact[12]	1.875	4.694	7.855	10.996	14.137	17.279	20.420	23.562	26.704	29.845

clamped boundary condition is simulated by a very stiff translational and rotational spring. The deflection of the beam can be expressed in the form of Fourier series as follows:

$$w(y,t) = q_1(t)(1) + q_2(t)\cos\omega_0 y + q_3(t)\sin\omega_0 y + \cdots + q_{2r}(t)\cos r\omega_0 y + q_{2r+1}(t)\sin r\omega_0 y \tag{6}$$

For illustration, a 10th-order Fourier series is used, that is, $r = 10$ ($R = 21$). The Gibbs phenomenon is demonstrated by evaluating the vibration frequencies using various basic frequencies ω_0 ranging from $0.5\pi/L$ to $2.0\pi/L$, that is, various periods T ($T = 2\pi/\omega_0$) ranging from $4L$ to L. The computed results are shown in Table 1, in which the vibration frequencies are expressed in dimensionless form such that $\beta_j = l\sqrt[4]{(\rho A\omega_j^2/EI)}$.

It can be seen from Table 1 that using a Fourier expansion with direct periodic extension with a period $T = l$ ($\omega_0 = 2.0\pi/L$) yields incorrect results. Also, results obtained from those with a period approaching $T = l$, that is, $\omega_0 = 1.75\pi/L$, also deviate markedly, in particular for the lower vibration frequencies. This demonstrates the Gibbs phenomenon occurring at the boundaries. On the other hand, using a Fourier expansion with indirect periodic extension with a period $T = 2l$ ($\omega_0 = \pi/L$) yields almost the exact solution.[12] Note that other periods in the range of $1.33l \le T \le 4l$ ($1.5\pi/L \ge \omega_0 \ge 0.5\pi/L$) also lead to good results. This is not surprising. In the present formulation, the period $T = 2l$ is chosen so that a conveniently equal-sized domain $[-l, 0]$ can provide ample maneuvering space to fit in the virtual smooth function φ_0.

The base functions in the Fourier series in Eq. (5) can then be chosen as the basis for the assumed vibration/buckling modes such that

$$\bar{Y}_m(y) = \begin{cases} \cos i\omega_0 y, & m = 2i-1 \\ \sin i\omega_0 y, & m = 2i \end{cases} \qquad (i = 1, 2, \ldots, r;\ m = 1, 2, \ldots, R;\ R = 2r) \tag{7}$$

The function $\bar{Y}_m(y)$ is called the Fourier base function hereafter. At this juncture, one may wonder whether the choice of the present Fourier base function is computationally efficient. Apparently smart alternatives could be to use a Chebyshev polynomial or any other complete function as the base function. They would allow for imposing boundary conditions as needed without the need for first doubling the domain. In particular, the Chebyshev basis may be able to achieve a competitive computational speed through the use of a fast cosine transform together with an iterative eigenvalue solver. However, note that the present choice of the extended periodic smooth Fouier base function does not carry any computational penalty because all numerical evaluations are carried out over the original domain, not the augmented domain.

B. Piecewise Cubic Polynomials

To alleviate the Gibbs phenomenon at the intrinsic interior discontinuities, a piecewise cubic polynomial $\tilde{Y}_m(y)$ is introduced in each segment, which is bounded by two consecutive discontinuities. For an arbitrary jth segment between points j and $j+1$ (Figs. 4 and 5),

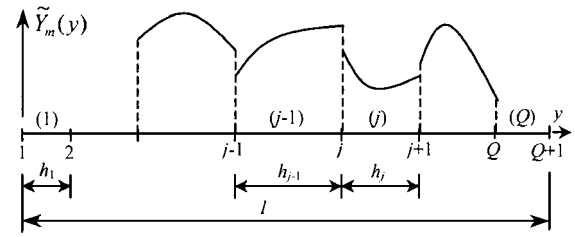

Fig. 4 Piecewise cubic polynomial functions.

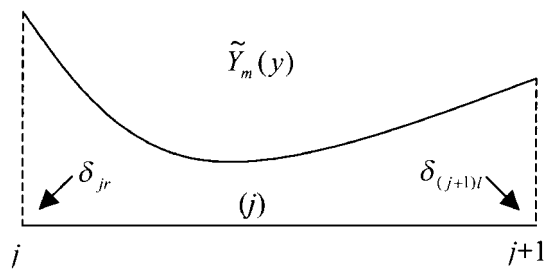

Fig. 5 Piecewise cubic polynomial function over a segment (y_j, y_{j+1}).

$$\tilde{Y}_m(y) = \boldsymbol{H}_{jr}(y)\delta_{jr} + \boldsymbol{H}_{(j+1)l}(y)\delta_{(j+1)l}, \qquad y \in (y_i, y_{j+1}) \tag{8}$$

in which

$$\boldsymbol{H}_{jr}(y) = [A_{jr}(y) \quad B_{jr}(y)] = \{[2(y-y_j)/h_j + 1] \times [1-(y-y_j)/h_j]^2\,(y-y_j)[1-(y-y_j)/h_j]\} \tag{9}$$

$$\boldsymbol{H}_{(j+1)l}(y) = [A_{(j+1)l}(y) \quad B_{(j+1)l}(y)] = \{[(-2(y-y_j)/h_j + 3] \times [(y-y_j)/h_j]^2\,(y-y_j-h_j)[(y-y_j)/h_j]\} \tag{10}$$

$$\delta_{jr} = [R_j \quad R'_j]^T \tag{11}$$

$$\delta_{(j+1)l} = [L_{j+1} \quad L'_{j+1}]^T \tag{12}$$

where R_j and R'_j, respectively, are the value and the first derivative of the function $\tilde{Y}_m(y)$ at point y_j^+ [right-hand side (RHS) of y_j]; L_{j+1} and L'_{j+1}, respectively, are the value and the first derivative of the function $\tilde{Y}_m(y)$ at point y_{j+1}^- [left-hand side (LHS) of y_{j+1}]; whereas $\boldsymbol{H}_{jr}(y)$ and $\boldsymbol{H}_{(j+1)l}(y)$ are, respectively, the Hermitian interpolation base functions for the jth segment.

C. GPFFS Function

Combining the piecewise cubic polynomials in Eq. (8) with the Fourier base function in Eq. (7), we can obtain the final form of the representation function, namely, the GPFFS function:

$$Y_m(y) = \bar{Y}_m(y) + \tilde{Y}_m(y) \tag{13}$$

By choosing a proper piecewise cubic polynomial $\tilde{Y}_m(y)$, we can force the function $Y_m(y)$ to satisfy all of the interior discontinuity conditions and any specific boundary conditions.

1. Interior Discontinuity Conditions (at $y = y_j$, $j = 2, 3, \ldots, Q$)

Open crack. For an open crack located at $y = y_j$, the continuity requirements are

$$R_j = L_j \tag{14}$$

$$R'_j = L'_j \tag{15}$$

$$R'''_j = L'''_j \tag{16}$$

and the discontinuity requirement[9] is

$$Y'_m(y_j + 0) - Y'_m(y_j - 0) = c_j Y''_m(y \to y_j) \tag{17}$$

where c_j is the flexibility coefficient of the crack with a depth of a_j. For one-sided cracks, it can be expressed as

$$c_j = 5.346 h(y_j) f(\xi_j) \qquad (j = 2, 3, \ldots, Q) \tag{18}$$

where $h(y_j)$ is the depth of the cross section of the beam at $y = y_j$ and

$$\xi_j = a_j / h(y_j) \tag{19}$$

$$f(\xi) = 1.8624\xi^2 - 3.95\xi^3 + 16.375\xi^4 - 37.226\xi^5 + 76.81\xi^6 - 126.9\xi^7 + 172\xi^8 - 143.97\xi^9 + 66.56\xi^{10} \tag{20}$$

Equation (17) can be written as

$$R'_j - L'_j = c_j [R''_j + \bar{Y}''_m(y_j)] \tag{21}$$

Through algebraic manipulations, Eqs. (14–16) and (21) can be written in matrix form as follows:

$$\boldsymbol{A}_j \begin{Bmatrix} \delta_{(j-1)r} \\ \delta_{jl} \\ \delta_{jr} \\ \delta_{(j+l)l} \end{Bmatrix} = \boldsymbol{b}_j \tag{22}$$

where

$$\boldsymbol{A}_j = \begin{bmatrix} 0 & 0 & -1 & 0 & 1 & 0 & 0 & 0 \\ 0 & 0 & 0 & -1 & 0 & 1 & 0 & 0 \\ -(I_{j-1}/I_j)A''_{(j-1)r} & -(I_{j-1}/I_j)B''_{(j-1)r} & -(I_{j-1}/I_j)A''_{jl} & -(I_{j-1}/I_j)B''_{jl} & A''_{jr} & B''_{jr} & A''_{(j+1)l} & B''_{(j+1)l} \\ -(I_{j-1}/I_j)A'''_{(j-1)r} & -(I_{j-1}/I_j)B'''_{(j-1)r} & -(I_{j-1}/I_j)A'''_{jl} & -(I_{j-1}/I_j)B'''_{jl} & A'''_{jr} & B'''_{jr} & A'''_{(j+1)l} & B'''_{(j+1)l} \end{bmatrix}_{y=y_j} \tag{35}$$

$$\boldsymbol{b}_j = [0 \quad 0 \quad 0 \quad c_j \bar{Y}''_m(y_j)]^T \tag{24}$$

Rigid support. For a rigid support located at $y = y_j$, the continuity requirements are

$$R_j = L_j \tag{25}$$

$$R'_j = L'_j \tag{26}$$

$$R''_j = L''_j \tag{27}$$

and the support condition is

$$L_j = -\bar{Y}_m(y_j) \tag{28}$$

Through algebraic manipulations, Eqs. (25–28) can be written in matrix form as Eq. (22) in which

$$\boldsymbol{A}_j = \begin{bmatrix} 0 & 0 & -1 & 0 & 1 & 0 & 0 & 0 \\ 0 & 0 & 0 & -1 & 0 & 1 & 0 & 0 \\ -A''_{(j-1)r} & -B''_{(j-1)r} & -A''_{jl} & -B''_{jl} & A''_{jr} & B''_{jr} & A''_{(j+1)l} & B''_{(j+1)l} \\ 0 & 0 & 0 & 0 & 1 & 0 & 0 & 0 \end{bmatrix}_{y=y_j} \tag{29}$$

$$\boldsymbol{b}_j = [0 \quad 0 \quad 0 \quad -\bar{Y}_m(y_j)]^T \tag{30}$$

Abrupt change of cross section. For an abrupt change of cross section at $y = y_j$, the continuity requirements are

$$R_j = L_j \tag{31}$$

$$R'_j = L'_j \tag{32}$$

and the discontinuity requirement is

$$R''_j + \bar{Y}''_m(y_j) = (I_{j-1}/I_j)[L''_j + \bar{Y}''_m(y_j)] \tag{33}$$

$$R'''_j + \bar{Y}'''_m(y_j) = (I_{j-1}/I_j)[L'''_j + \bar{Y}'''_m(y_j)] \tag{34}$$

Through algebraic manipulations, Eqs. (31–34) can be written in matrix form as Eq. (22) in which

$$\boldsymbol{b}_j = [0 \quad 0(I_{j-1}/I_j - 1)\bar{Y}''_m(y_j) \quad (I_{j-1}/I_j - 1)\bar{Y}'''_m(y_j)]^T \tag{36}$$

2. Boundary Conditions at $y = 0$ (LHS)

Similar relations can be obtained for different boundary conditions as follows.

Simply supported [$R_{1r} = -\bar{Y}_m(y_1)$, $R''_{1r} = -\bar{Y}''_m(y_1)$]:

$$\boldsymbol{A}_1 \begin{Bmatrix} \delta_{1r} \\ \delta_{2l} \end{Bmatrix} = \boldsymbol{b}_1 \tag{37}$$

$$\boldsymbol{A}_j = \begin{bmatrix} 0 & 0 & -1 & 0 & 1 & 0 & 0 & 0 \\ -A''_{(j-1)r} & -B''_{(j-1)r} & -A''_{jl} & -B''_{jl} & A''_{jr} & B''_{jr} & A''_{(j+1)l} & B''_{(j+1)l} \\ -A'''_{(j-1)r} & -B'''_{(j-1)r} & -A'''_{jl} & -B'''_{jl} & A'''_{jr} & B'''_{jr} & A'''_{(j+1)l} & B'''_{(j+1)l} \\ 0 & 0 & 0 & -1 & -c_j A''_{jr} & 1 - c_j B''_{jr} & -c_j A''_{(j+1)l} & -c_j B''_{(j+1)l} \end{bmatrix}_{y=y_j} \tag{23}$$

where

$$\boldsymbol{A}_1 = \begin{bmatrix} 1 & 0 & 0 & 0 \\ A''_{1r} & B''_{1r} & A''_{2l} & B''_{2l} \end{bmatrix}_{y=y_1} \tag{38}$$

$$\boldsymbol{b}_1 = \begin{bmatrix} -\bar{Y}_m(y_1) \\ -\bar{Y}''_m(y_1) \end{bmatrix} \tag{39}$$

Clamped support $[R_{1r} = -\bar{Y}_m(y_1),\ R'_{1r} = -\bar{Y}'_m(y_1)]$:

$$\boldsymbol{A}_1 = \begin{bmatrix} 1 & 0 & 0 & 0 \\ 0 & 1 & 0 & 0 \end{bmatrix} \tag{40}$$

$$\boldsymbol{b}_1 = \begin{bmatrix} -\bar{Y}_m(y_1) \\ -\bar{Y}'_m(y_1) \end{bmatrix} \tag{41}$$

Free end $[R''_{1r} = -\bar{Y}''_m(y_1),\ R'''_{1r} = -\bar{Y}'''_m(y_1)]$:

$$\boldsymbol{A}_1 = \begin{bmatrix} A''_{1r} & B''_{1r} & A''_{2l} & B''_{2l} \\ A'''_{1r} & B'''_{1r} & A'''_{2l} & B'''_{2l} \end{bmatrix}_{y=y_1} \tag{42}$$

$$\boldsymbol{b}_1 = \begin{bmatrix} -\bar{Y}''_m(y_1) \\ -\bar{Y}'''_m(y_1) \end{bmatrix} \tag{43}$$

3. Boundary Conditions $y = l$ (RHS)

Similar relations can be obtained for different boundary conditions as follows.

Simply supported $[L_{Q+1} = -\bar{Y}_m(y_{Q+1}),\ L''_{Q+1} = -\bar{Y}''_m(y_{Q+1})]$:

$$\boldsymbol{A}_{Q+1} \begin{Bmatrix} \delta_{Qr} \\ \delta_{(Q+1)l} \end{Bmatrix} = \boldsymbol{b}_{Q+1} \tag{44}$$

where

$$\boldsymbol{A}_{Q+1} = \begin{bmatrix} 0 & 0 & 1 & 0 \\ A''_{Qr} & B''_{Qr} & A''_{(Q+1)l} & B''_{(Q+1)l} \end{bmatrix}_{y=y_{Q+1}} \tag{45}$$

$$\boldsymbol{b}_{Q+1} = \begin{bmatrix} -\bar{Y}_m(y_{Q+1}) \\ -\bar{Y}''_m(y_{Q+1}) \end{bmatrix} \tag{46}$$

Clamped support $[L_{Q+1} = -\bar{Y}_m(y_{Q+1}),\ L'_{Q+1} = -\bar{Y}'_m(y_{Q+1})]$:

$$\boldsymbol{A}_{Q+1} = \begin{bmatrix} 1 & 0 & 0 & 0 \\ 0 & 1 & 0 & 0 \end{bmatrix} \tag{47}$$

$$\boldsymbol{b}_{Q+1} = \begin{bmatrix} -\bar{Y}_m(y_{Q+1}) \\ -\bar{Y}'_m(y_{Q+1}) \end{bmatrix} \tag{48}$$

Free end $[L''_{Q+1} = -\bar{Y}''_m(y_{Q+1}),\ L'''_{Q+1} = -\bar{Y}'''_m(y_{Q+1})]$:

$$\boldsymbol{A}_{Q+1} = \begin{bmatrix} A''_{Qr} & B''_{Qr} & A''_{(Q+1)l} & B''_{(Q+1)l} \\ A'''_{Qr} & B'''_{Qr} & A'''_{(Q+1)l} & B'''_{(Q+1)l} \end{bmatrix}_{y=y_{Q+1}} \tag{49}$$

$$\boldsymbol{b}_{Q+1} = \begin{bmatrix} -\bar{Y}''_m(y_{Q+1}) \\ -\bar{Y}'''_m(y_{Q+1}) \end{bmatrix} \tag{50}$$

4. Combined Expression

All of the interior continuity/discontinuity requirements and boundary conditions can be grouped together and written in one single matrix equation as follows:

$$\boldsymbol{A}\boldsymbol{x} = \boldsymbol{b} \tag{51}$$

where

$$\boldsymbol{A} = \begin{bmatrix} \boldsymbol{A}_1 & 0 & \cdots & \cdots & 0 \\ 0 & \boldsymbol{A}_2 & \cdots & \cdots & 0 \\ 0 & \cdots & \cdots & \cdots & 0 \\ 0 & \cdots & \cdots & \boldsymbol{A}_Q & 0 \\ 0 & \cdots & \cdots & \cdots & \boldsymbol{A}_{Q+1} \end{bmatrix} \tag{52}$$

$$\boldsymbol{x} = [\delta_{1r} \quad \delta_{2l} \quad \delta_{2r} \quad \delta_{3l} \quad \delta_{3r} \quad \cdots \quad \delta_{Ql} \quad \delta_{Qr} \quad \delta_{(Q+1)l}]^T \tag{53}$$

$$\boldsymbol{b} = [\boldsymbol{b}_1 \quad \boldsymbol{b}_2 \quad \cdots \quad \boldsymbol{b}_Q \quad \boldsymbol{b}_{Q+1}]^T \tag{54}$$

Solving Eq. (51), we can obtain the piecewise cubic polynomial and, thus, determine the final GPFFS function.

III. Vibration and Buckling Analysis of Complex Beams

A. Vibration of Cracked Beam

A beam with cracks at locations $y = y_j$, $j = 2, \ldots, Q$ (Fig. 1), can be modeled as a beam having Q segments delineated by the cracks. Any two neighboring segments are inter-connected by a massless rotational spring, which is planted to simulate the effect of the crack. The vibration modes of the cracked beam should be C^0 continuous and, therefore, are represented by the corresponding C^0 GPFFS functions. Results are obtained through energy formulations.

1. Potential Energy U

The potential energy of the cracked beam can be expressed as the sum of two components:

$$U = U_1 + U_2 \tag{55}$$

in which U_1 is the potential energy stored in the cracked beam due to the bending deformation of the beam itself; U_2 is the potential energy stored in the massless rotational springs that are used to model the effects of crack(s).

To express U_1 and U_2 in a concise way, we denote

$$\bar{\boldsymbol{Y}}(y) = [\bar{Y}_1(y) \quad \bar{Y}_2(y) \quad \cdots \quad \bar{Y}_R(y)] \tag{56}$$

$$\tilde{\boldsymbol{Y}}(y) = [\tilde{Y}_1(y) \quad \tilde{Y}_2(y) \quad \cdots \quad \tilde{Y}_R(y)] \tag{57}$$

$$\boldsymbol{Y}(y) = [Y_1(y) \quad Y_2(y) \quad \cdots \quad Y_R(y)] \tag{58}$$

$$\boldsymbol{q}(t) = [q_1(t) \quad q_2(t) \quad \cdots \quad q_R(t)]^T \tag{59}$$

Thus, we have

$$\boldsymbol{Y}(y) = \bar{\boldsymbol{Y}}(y) + \tilde{\boldsymbol{Y}}(y) \tag{60}$$

$$w(y, t) = \boldsymbol{Y}(y)\boldsymbol{q}(t) \tag{61}$$

Then we can derive the expressions for the energy terms U_i as follows.

Potential energy U_1:

$$U_1 = \sum_{i=1}^{Q} \frac{1}{2} \int_{y_i}^{y_{i+1}} EI(y) w^2_{,yy}(y, t)\, \mathrm{d}y \tag{62}$$

Substituting Eq. (61) into Eq. (62) yields

$$U_1 = \tfrac{1}{2}\boldsymbol{q}^T \boldsymbol{K}_1 \boldsymbol{q} \tag{63}$$

where $\boldsymbol{K}_1$ represents the stiffness matrix of the cracked beam corresponding to the potential energy U_1 such that

$$\boldsymbol{K}_1 = \sum_{i=1}^{Q} \int_{y_i}^{y_{i+1}} EI(y) \boldsymbol{Y}^T_{,yy}(y) \boldsymbol{Y}_{,yy}(y)\, \mathrm{d}y \tag{64}$$

Potential energy U_2:

$$U_2 = \sum_{j=2}^{Q} \frac{1}{2}\left[\frac{EI(y_j)}{c_j}\right][w_{,y}(y_j + 0, t) - w_{,y}(y_j - 0, t)]^2 \quad (65)$$

Substituting Eq. (61) into Eq. (65) yields

$$U_2 = \tfrac{1}{2}\boldsymbol{q}^T \boldsymbol{K}_2 \boldsymbol{q} \quad (66)$$

where $\boldsymbol{K}_2$ is the stiffness matrix of the cracked beam corresponding to the potential energy U_2 such that

$$\boldsymbol{K}_2 = \sum_{j=2}^{Q} [c_{j-1} EI(y_j)] \boldsymbol{Y}_{,yy}^T(y_j) \boldsymbol{Y}_{,yy}(y_j) \quad (67)$$

Subsequently, substituting Eqs. (63) and (66) into Eq. (55) yields the relation for the total potential energy of the cracked beam:

$$U = \tfrac{1}{2}\boldsymbol{q}^T \boldsymbol{K} \boldsymbol{q} \quad (68)$$

where $\boldsymbol{K}$ is the sum of the two component stiffness matrices, that is,

$$\boldsymbol{K} = \boldsymbol{K}_1 + \boldsymbol{K}_2 \quad (69)$$

2. Kinetic Energy T

The kinetic energy T of the cracked beam can be expressed as

$$T = \frac{1}{2}\int_0^l \rho A(y) w_{,t}^2(y, t)\, \mathrm{d}y \quad (70)$$

Substituting Eq. (61) into Eq. (70) yields

$$T = \tfrac{1}{2}\dot{\boldsymbol{q}}^T \boldsymbol{M} \dot{\boldsymbol{q}} \quad (71)$$

where $\boldsymbol{M}$ is the mass matrix of the cracked beam such that

$$\boldsymbol{M} = \int_0^1 \rho A(y) \boldsymbol{Y}^T(y) \boldsymbol{Y}(y)\, \mathrm{d}y \quad (72)$$

3. Vibration Equation

By using the Euler–Lagrangian equation, we can obtain the free vibration equation and, thus, the frequency equation of the complex beam as follows:

$$\boldsymbol{K}\boldsymbol{q} = \omega^2 \boldsymbol{M}\boldsymbol{q} \quad (73)$$

or

$$(\boldsymbol{K}_1 + \boldsymbol{K}_2)\boldsymbol{q} = \omega^2 \boldsymbol{M}\boldsymbol{q} \quad (74)$$

Solving the eigenvalue equation yields the vibration frequencies. Note that the employment of the C^0 GPFFS function results in reduction of frequencies compared to those for a similar but uncracked perfect beam.

B. Buckling of Cracked Beam

Similar to the vibration problems, the buckling load of a cracked beam can be obtained through energy formulations.

1. Geometrical Stiffness Matrix

The potential energy due to a variable axial load $\lambda N(y)$ can be expressed as

$$U_3 = -\frac{1}{2}\lambda \int_0^l N(y)[w_{,y}(y, t)]^2\, \mathrm{d}y \quad (75)$$

In the special case of constant axial load P, we can simply set $\lambda = P$ and $N(y) = 1$. Substituting Eq. (61) into Eq. (75) yields

$$U_3 = -\tfrac{1}{2}\lambda \boldsymbol{q}^T \boldsymbol{K}_G \boldsymbol{q} \quad (76)$$

where

$$\boldsymbol{K}_G = \int_0^l N(y) \boldsymbol{Y}_{,y}^T(y) \boldsymbol{Y}_{,y}(y)\, \mathrm{d}y \quad (77)$$

2. Buckling Equation

The buckling equation can then be written as

$$(\boldsymbol{K}_1 + \boldsymbol{K}_2)\boldsymbol{q} = \lambda \boldsymbol{K}_G \boldsymbol{q} \quad (78)$$

The lowest eigenvalue λ obtained from Eq. (78), therefore, gives the buckling load P, and the associated eigenvector $\boldsymbol{q}$ is the generalized buckling mode.

Equations (74) and (78) are typical linear eigenvalue equations. Apparently, they can be solved using a standard dense matrix QZ solver. In the examples shown in Sec. V, the problem size is small, and the solutions are obtained using the subspace iteration method. In practical applications, many of the vibration/buckling dynamic analyses produce a sparse set of stiffness and mass system of equations. Solving a large linear system of equations requires an efficient robust eigensolver. Very often, the Lancos method tends to be more robust and faster than subspace methods.

IV. Extension to Two- and Three-Dimensional Problems

The presented method can be extended to two- and three-dimensional problems. A simple way is to extend the function $f(y, t)$ to $f(x, y, t)$ in the two-dimensional case or to $f(x, y, z, t)$ in the three-dimensional case through simple tensor product. For example, in the three-dimensional case,

$$f(x, y, z, t) = \sum_{m=1}^{R_1}\sum_{n=1}^{R_2}\sum_{p=1}^{R_3} X_m(x) Y_n(y) Z_p(z) q_{mnp}(t) \quad (79)$$

where X_m, Z_p, and $q_{mnp}(t)$ are defined in the same manner as in the one-dimensional case.

However, the function defined by Eq. (79) represents a homogeneous condition at any interior section as well as the boundaries. Also its applications are limited to those problems defined in a rectangular box-shape domain.

To alleviate these limitations, a weak form in other direction(s) can be adopted. The present one-dimensional function is a strong form. It can be used directly in combination with the partial discretization technique exemplified in the finite strip[13] method or the finite layer[14] method, which are varieties of the versatile finite element method. Hence, the scope of its applications can be broadened.

V. Numerical Examples

Example 1: Free Vibration of a Cantilever Beam with an Open Crack Near its Clamped End

A cantilevered beam with a crack near its clamped end is considered. The results obtained from the present method (using $r = 5$) and those given by Shifrin et al.[9] are shown in Fig. 6. The vertical axis stands for the ratio of the natural frequency of the cracked beam to that of an uncracked beam, that is, the frequency reduction. The horizontal axis stands for the normalized stiffness (l/c_1) of the artificial rotational spring introduced at the crack. Note that the present results agree perfectly with those by Shifrin and Ruotolo,[9] who obtained the results by solving the governing differential equations segmentally.

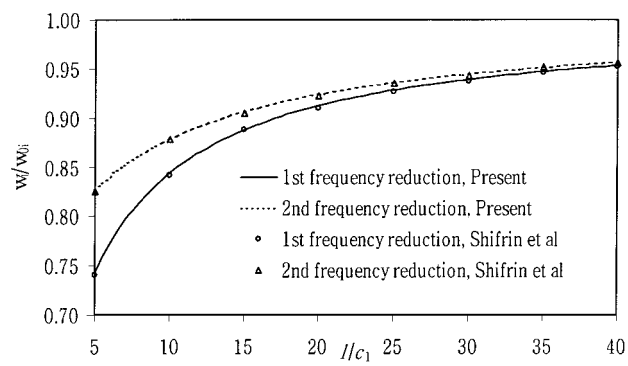

Fig. 6 Frequency reduction of a cantilever beam with an open crack at its clamped end.

Table 2 Natural frequencies of a clamped beam stiffened by rings

			Dube et al.[10]			Present method		
n_r	r_{EI}	r_{ba}	β_1	β_2	β_3	β_1	β_2	β_3
0	4	0.10	3.516	22.03	61.70	3.5160	22.0345	61.6972
1	4	0.10	4.029	24.92	68.81	4.0291	24.9174	68.8145
2	4	0.10	3.667	21.85	65.61	3.6666	21.8468	65.6128
4	4	0.10	3.445	21.49	59.68	3.4450	21.4861	59.6845
6	4	0.10	3.372	21.10	58.97	3.3718	21.0960	58.9679
1	4	0.00	3.516	22.03	61.70	3.5160	22.0345	61.6972
1	4	0.10	4.029	24.92	68.81	4.0291	24.9174	68.8145
1	4	0.20	4.504	26.71	69.37	4.5040	26.7062	69.3747
1	1	0.15	3.516	22.03	61.70	3.5160	22.0345	61.6972
1	2	0.15	3.971	24.10	65.56	3.9705	24.0995	65.5625
1	4	0.15	4.272	25.97	70.14	4.2722	25.9712	70.1383
1	6	0.15	4.388	26.84	72.74	4.3883	26.8350	72.7415

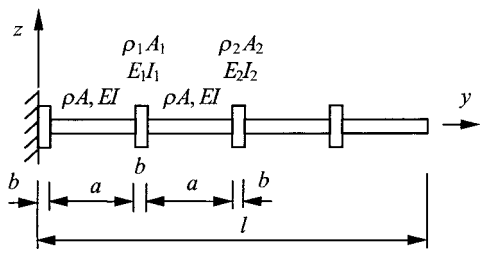

Fig. 7 Cantilever beam/column stiffened by rings.

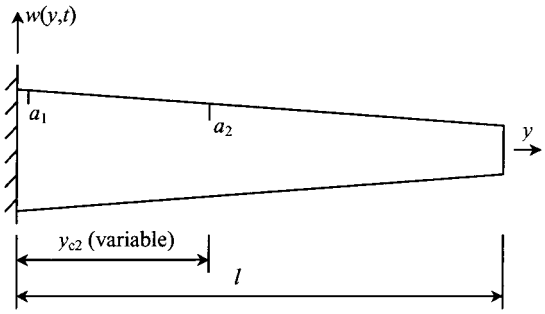

Fig. 8 Nonuniform cantilever beam with two open cracks.

Example 2: Free Vibration of a Cantilever Beam with Stiffening Rings

Figure 7 shows a cantilever beam with stiffening rings. The stiffening rings with the same width b are at regular spacing $(a+b)$. The symbol n_r denotes the number of rings. The ratio of the flexural rigidity of the ring to that of the beam is $r_{EI} = E_1 I_1 / EI$, and the corresponding ratio for the masses is $\gamma = \rho_1 A_1 / \rho A$. The ratio of b to a is $r_{ba} = b/a$. The free vibration of a beam (with $\gamma = r_{EI}$) is analyzed by using a fifth-order $(r=5)$ GPFFS function. The natural angular frequency ω was made dimensionless using the expression $\beta_i = l^2\sqrt{(\rho A/EI)}\omega_i$. The lowest three dimensionless frequencies are shown in Table 2 and compared to those given by Dube et al.,[10] who solved the governing differential equations segmentally. Perfect agreement is observed.

Example 3: Buckling Load of a Cantilever Column with Stiffening Rings

A column having the same configuration as the beam shown in Fig. 7 $(\gamma = r_{EI})$ is reanalyzed but is now subjected to an axial load. In the stability analysis, a fifth-order $(r=5)$ GPFFS function is used. The buckling load P_{cr} is made dimensionless using the expression $P^*_{cr} = P_{cr} l^2 / EI$. The dimensionless buckling loads P^*_{cr} are shown in Table 3 and compared to those given by Dube et al.[10] Again, perfect agreement is observed.

Example 4: Natural Frequencies of a Nonuniform Beam with Two Open Cracks

Figure 8 shows a nonuniform cantilevered beam with two open cracks. The beam has a rectangular crosssection with constant width b but linearly varying height $h(y)$. The following parameters are used: $l = 1.2$ m (3.94 ft), $b = 0.02$ m (0.066 ft), and $h_1 = 0.04$ m (0.132 ft) (at the clamped end); $h_2 = 0.02$ m (0.066 ft) (at the free end); Young's modulus $E = 210$ GPa (30.46E6 psi); Poisson's ratio $\mu = 0.3$; and mass density $\rho = 7800$ kg/m^3 (15.13 slug/ft^3). The first crack of depth $a_1 = 0.02$ m (0.066 ft) is located at the clamped end. The second crack of depth $a_2 = 0.01$ m (0.033 ft) has variable locations changing from $y = 0.01$ to 1.1 m (0.033 to 3.61 ft). The frequency reductions versus the locations of the second crack are shown in Fig. 9.

Table 3 Buckling loads of a cantilever column stiffened by rings

			P^*_{cr}	
n_r	r_{EI}	r_{ba}	Dube et al.[10]	Present
0	4	0.10	2.467	2.4675
1	4	0.10	2.842	2.8416
2	4	0.10	2.739	2.7388
3	4	0.10	2.708	2.7078
4	4	0.10	2.692	2.6926
6	4	0.10	2.678	2.6776
8	4	0.10	2.670	2.6702
10	4	0.10	2.666	2.6657
1	4	0.0	2.467	2.4675
1	4	0.05	2.654	2.6536
1	4	0.10	2.842	2.8416
1	4	0.15	3.031	3.0309
1	4	0.20	3.221	3.2212
1	1	0.15	2.467	2.4675
1	2	0.15	2.822	2.8222
1	4	0.15	3.031	3.0309
1	6	0.15	3.106	3.1057
1	10	0.15	3.167	3.1674
1	1000	0.15	3.262	3.2624

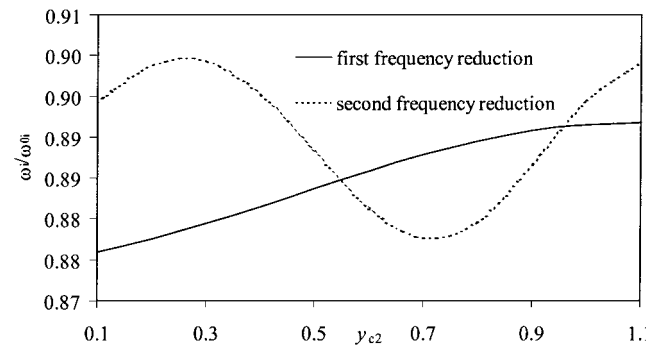

Fig. 9 Effect of locations of a second crack on frequency reduction of a nonuniform beam with two cracks.

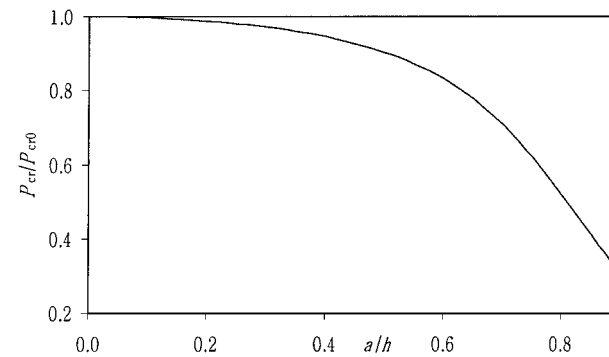

Fig. 10 Effect of depths of a crack on the buckling load of a cantilever column with a crack near its base.

Example 5: Buckling Load of a Cantilever Column with an Open Crack near Its Base

Consider a cantilever column with an open crack near its base. The depth a of the crack is variable. The column has a square cross section of width b, and its height is l. The following parameters are used: $l = 1.0$ m (3.28 ft), $b = 0.02$ m (0.066 ft), $E = 210$ GPa (30.46E6 psi), and $\mu = 0.3$. The buckling-load reductions vs the depth ratios (a/h) of the crack are shown in Fig. 10.

VI. Conclusions

A kind of GPFFS function was presented. When these GPFFS functions were used as representation functions for some physical parameters such as the deflection shapes of a beam or column having some intrinsic discontinuities, the undesirable Gibbs phenomena can be eliminated. In addition, the inherent discontinuities at the boundaries arising from the Fourier series are also eliminated. Consequently, Gibbs phenomena are eliminated for the whole domain including the boundaries. Its versatility and robustness were demonstrated in its applications in the vibration and buckling analysis of complex beams.

References

[1]Tadikonda, S. S. K., and Baruh, H., "Gibbs Phenomenon in Structural Mechanics," *AIAA Journal*, Vol. 29, No. 9, 1991, pp. 1488–1497.

[2]Thurston, G. A., and Sistla, R., "Elimination of Gibbs' Phenomenon from Error Analysis of Finite Element Results," *AIAA Journal*, Vol. 29, No. 12, 1991, pp. 2233–2239.

[3]Gottlieb, D., and Shu, C. W., "On the Gibbs Phenomenon and Its Resolution," *Society for Industrial and Applied Mathematics Review*, Vol. 39, No. 4, 1997, pp. 644–668.

[4]Kabir, H. R. H., and Chaudhuri, R. A., "On Gibbs-Phenomenon-Free Fourier Solution for Finite Shear-Flexible Laminated Clamped Curved Panels," *International Journal for Mechanical Sciences*, Vol. 32, No. 2, 1994, pp. 501–520.

[5]Gelb, A., and Gottlieb, D., "Resolution of the Gibbs Phenomenon for 'Spliced' Functions in One and Two Dimensions," *Computers and Mathematics with Applications*, Vol. 33, No. 11, 1997, pp. 35–38.

[6]Zhang, Z. M., and Martin, C. F., "Convergence and Gibbs' Phenomenon in Cubic Spline Interpolation of Discontinuous Functions," *Journal of Computational and Applied Mathematics*, Vol. 87, No. 2, 1997, pp. 359–371.

[7]Liu, J. Y., Zheng, D. Y., and Mei, Z. J., "Practical Integral Transforms in Engineering," Huazhong Univ. of Science and Technology Press, Wuhan, PRC, 1995 (in Chinese).

[8]Zheng, D. Y., "Vibration and Stability Analysis of Plate-Type Structures under Moving Loads by Analytical and Numerical Methods," Ph.D. Dissertation, Dept. of Civil Engineering, Univ. of Hong Kong, Hong Kong, PRC, June 1999.

[9]Shifrin, E. I., and Ruotolo, R., "Natural Frequencies of a Beam with an Arbitrary Number of Cracks," *Journal of Sound and Vibration*, Vol. 222, No. 3, 1999, pp. 409–423.

[10]Dube, G. P., Agarwal, R. K., and Dumir, P. C., "Natural Frequencies and Buckling Loads of Beam-Columns Stiffened by Rings," *Applied Mathematical Modeling*, Vol. 20, No. 9, 1996, pp. 646–653.

[11]Au, F. T. K., Zheng, D. Y., and Cheung, Y. K., "Vibration and Stability of Non-Uniform Beams with Abrupt Changes of Cross-Section by Using C^1 Modified Beam Vibration Functions," *Applied Mathematical Modeling*, Vol. 29, No. 1, 1999, pp. 19–34.

[12]Gorman, D. J., *Free Vibration Analysis of Beams and Shafts*, Wiley, New York, 1975, p. 8.

[13]Cheung, Y. K., and Tham, L. G., *Finite Strip Method*, CRC Press, Boca Raton, FL, 1998, pp. 137–157.

[14]Cheung, Y. K., and Fan, S. C., "Analysis of Pavements and Layered Foundations by Finite Layer Method," *Proceedings of the Third International Conference on Numerical Methods in Geomechanics*, Vol. 3, A. A. Balkema Publishers, Rotterdam, The Netherlands, 1979, pp. 1129–1135.

A. Berman
Associate Editor